Supplementary Information

Converting detrimental HF in electrolyte into a highly-fluorinated interphase on cathode

Changchun Ye,[a,d] Wenqiang Tu,[a,d] Limei Yin,[a] Qinfeng Zheng,[a] Cun Wang,[a] Yaotang Zhong,[a] Yuegang Zhang,[a,b] Qiming Huang,[a,b] Kang Xu*[c] and Weishan Li*[a,b]

[a] School of Chemistry and Environment, South China Normal University, Guangzhou 510006, China. *E-mail: liwsh@scnu.edu.cn

[b] Engineering Research Center of MTEES (Ministry of Education), Research Center of BMET (Guangdong Province), Engineering Lab. of OFMHEB (Guangdong Province), Key Lab. of ETESPG(GHEI), and Innovative Platform for ITBMD (Guangzhou Municipality), South China Normal University, Guangzhou 510006, China.

[c] Electrochemistry Branch, Sensor and Electron Devices Directorate, Power and Energy Division, U.S. Army Research Laboratory, Adelphi, MD 20783, USA. *E-mail: conrad.k.xu.civ@mail.mil

[d] These authors contributed equally to this work.

Figure caption:

Fig. S1. Optimized structures of solvents (EC, EMC and DEC) and APTS.

Fig. S2. Optimized structures and adiabatic ionization energy (AIE, kJ mol^{-1}) of X (a), X-PF_6^- (b), X-HF (c), X- H^+ (d), and X-F^- (e), (X = EC, EMC, DEC, APTS) after one electron oxidation.

Fig. S3. SEM images of $Li_{1.2}Mn_{0.55}Ni_{0.15}Co_{0.1}O_2$ electrodes cycled in the STD (a) and APTS-containing (b) electrolytes containing 600 ppm.

Fig. S4. Discharge curves and corresponding dQ/dV profiles of $Li_{1.2}Mn_{0.55}Ni_{0.15}Co_{0.1}O_2$ electrodes in the STD (a and b) and APTS-containing (c and d) electrolytes at the selected cycles of Fig. 1.

Fig. S5. Experimental and fitted electrochemical impedance spectra of $Li_{1.2}Mn_{0.55}Ni_{0.15}Co_{0.1}O_2$ electrodes after 3 cycles (a) and 300 cycles (b) under the same charge/discharge conditions as Fig. 1; the fitted resistances (c) and the equivalent circuit (d) for fitting.

Fig. S6. XRD patterns of fresh and the cycled $Li_{1.2}Mn_{0.55}Ni_{0.15}Co_{0.1}O_2$ electrodes in the STD and APTS-containing electrolytes.

Fig. S7. Deposited transition metal on the Li counter electrode after cycling Li/ $Li_{1.2}Mn_{0.55}Ni_{0.15}Co_{0.1}O_2$ cells in the STD and APTS-containing electrolytes for 300 cycles.

Fig. S8. Voltage decaying curves (a) and chronoamperometric profiles at 4.8 V (b) for charged $Li_{1.2}Mn_{0.55}Ni_{0.15}Co_{0.1}O_2$ electrodes after three charge-discharge cycles at 0.1 C in the STD and APTS-containing electrolytes.

Fig. S9. FTIR spectra of fresh $Li_{1.2}Mn_{0.55}Ni_{0.15}Co_{0.1}O_2$ electrode and the electrodes after cycling test in Fig. 1 for STD and APTS-containing electrolytes.

Fig. S10. Cyclic performance (a), corresponding Coulombic efficiency (b) and initial charge-discharge profiles (c) of Li/graphite cells in the STD and APTS-containing electrolytes.

Fig. S11. Cyclic performance (a), corresponding Coulombic efficiency (b) and initial charge-discharge profiles (c) of graphite/$Li_{1.2}Mn_{0.55}Ni_{0.15}Co_{0.1}O_2$ cells in the STD APTS-containing electrolytes.

Fig. S12. Cyclic performance of fresh Li/pre-cycled $Li_{1.2}Mn_{0.55}Ni_{0.15}Co_{0.1}O_2$ and pre-cycled Li/fresh $Li_{1.2}Mn_{0.55}Ni_{0.15}Co_{0.1}O_2$ cells in the STD electrolyte at 1C between 2 V and 4.8 V.

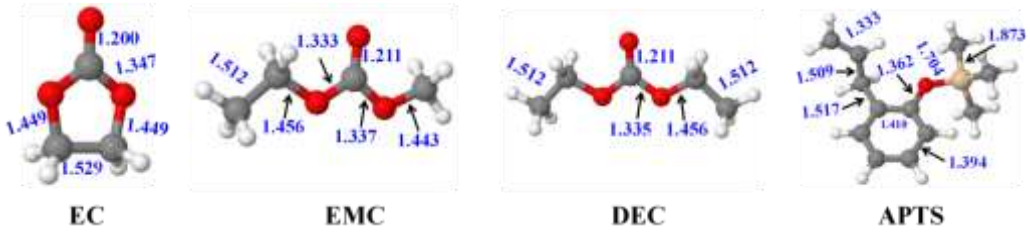

Fig. S1. Optimized structures of solvents (EC, EMC and DEC) and APTS.

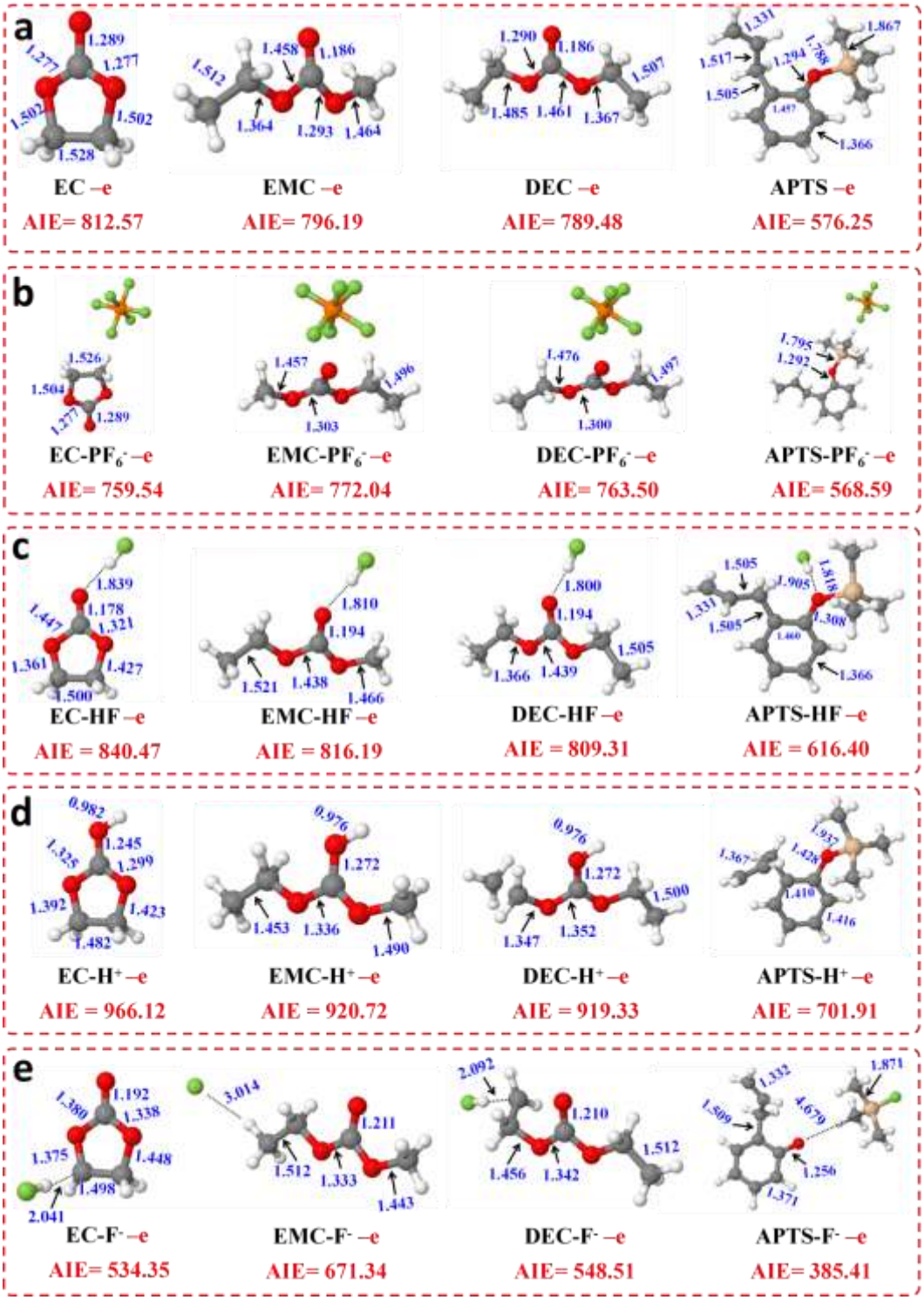

Fig. S2. Optimized structures and adiabatic ionization energy (AIE, kJ mol^{-1}) of X (a), X-PF_6^- (b), X-HF (c), X- H^+ (d), and X-F^- (e), (X = EC, EMC, DEC, APTS) after one electron oxidation.

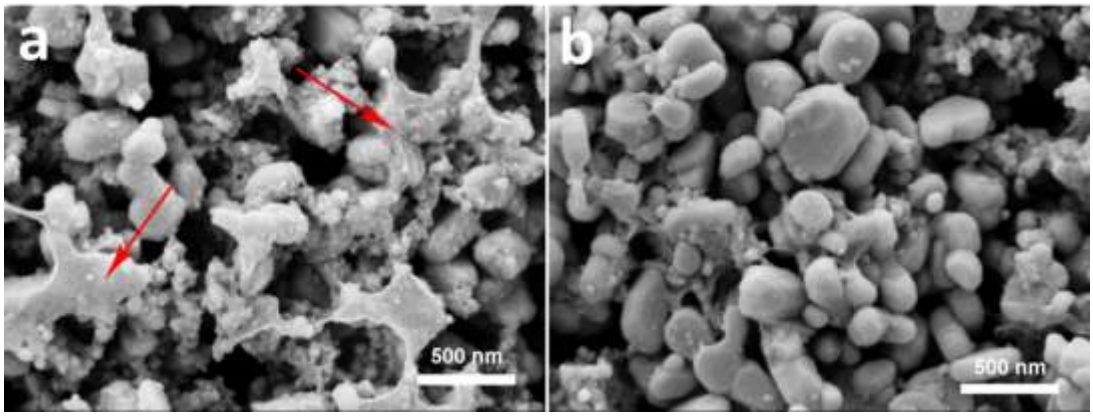

Fig. S3. SEM images of $Li_{1.2}Mn_{0.55}Ni_{0.15}Co_{0.1}O_2$ electrodes cycled in the STD (a) and APTS-containing (b) electrolytes containing 600 ppm.

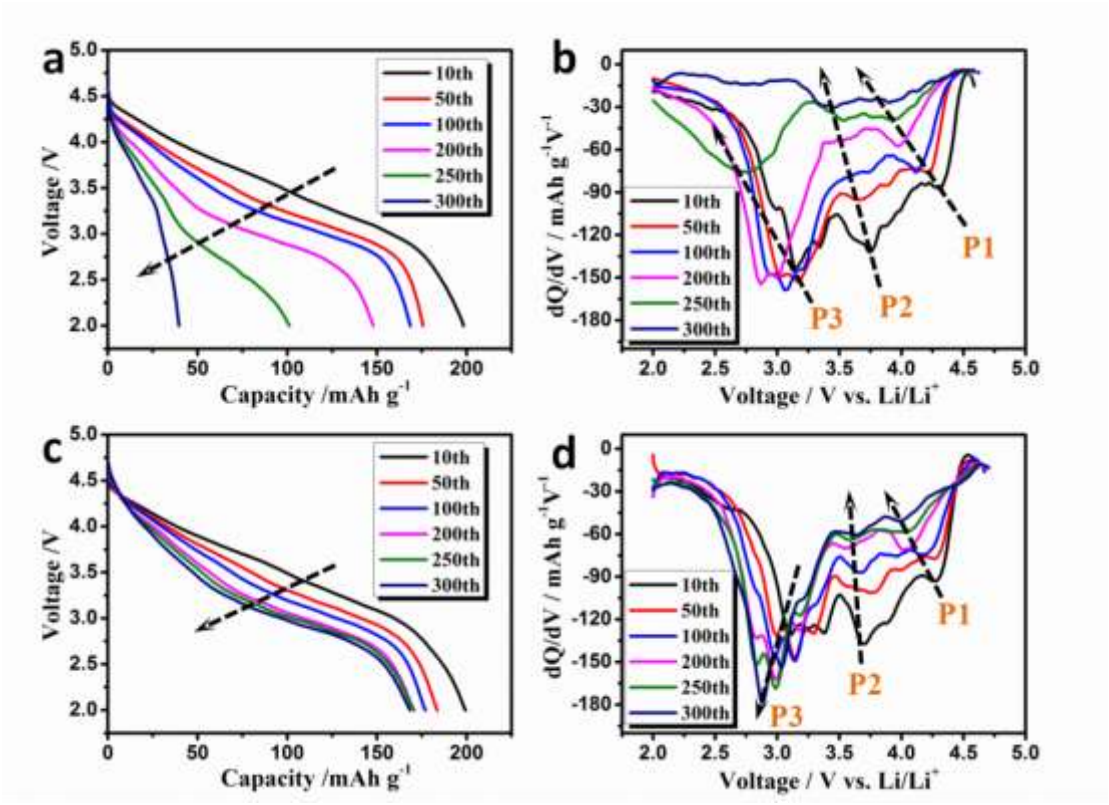

Fig. S4. Discharge curves and corresponding dQ/dV profiles of $Li_{1.2}Mn_{0.55}Ni_{0.15}Co_{0.1}O_2$ electrodes in the STD (a and b) and APTS-containing (c and d) electrolytes at the selected cycles of Fig. 1.

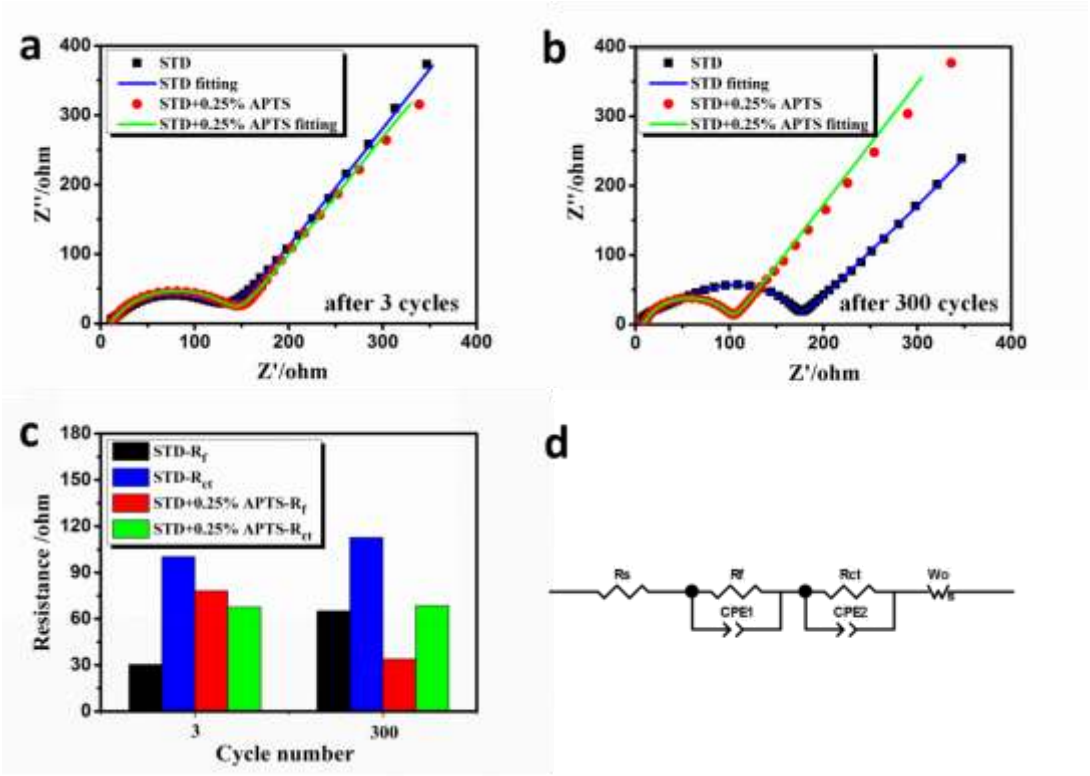

Fig. S5. Experimental and fitted electrochemical impedance spectra of $Li_{1.2}Mn_{0.55}Ni_{0.15}Co_{0.1}O_2$ electrodes after 3 cycles (a) and 300 cycles (b) under the same charge/discharge conditions as Fig. 1; the fitted resistances (c) and the equivalent circuit (d) for fitting.

The pressed semicircle in the impedance spectra represents the interfacial impedance including the lithium transportation impedance in the film and the charge transfer impedance on the interphase, while the slope line reflects the lithium diffusion in the electrode.[1, 2] The experimental impedance spectra can be well fitted by equivalent circuit of **Fig. S**5d, which includes the resistances of the Ohmic, the film (R_f) and the charge transfer (R_{ct}), and Warburg impedance (W_o). The larger R_f of LMR after 3 cycles in the APTS-containing electrolyte than that in the STD electrolyte (**Fig. S5**c), suggests the formation of a protective interphase film by APTS, which is beneficial for the charge transfer (smaller R_{ct}). After 300 cycles, the R_f of LMR in the APTS-containing electrolyte becomes smaller and its R_{ct} changed little, suggesting that the film might experience a structural re-organization, which is beneficial for the lithium ion transportation and does not affect the charge transfer process. However, both R_f and R_{ct} of LMR after long cycling in the STD electrolyte

increases significantly, suggesting that LMR suffer a structural destruction. Apparently, the film formed form APTS provides a protection for the structural integrity.

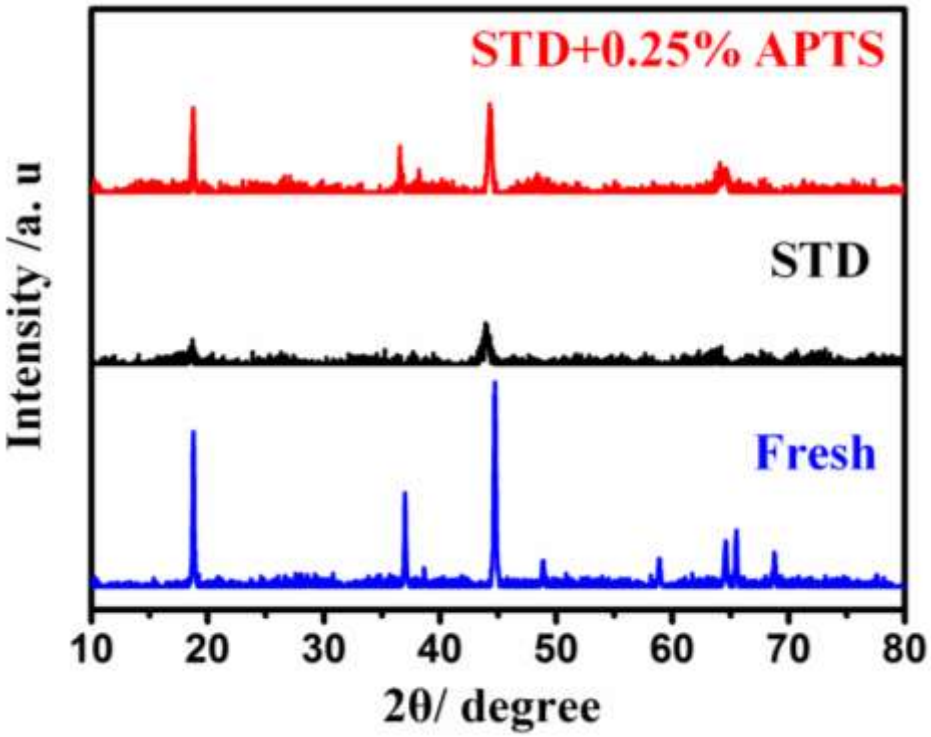

Fig. S6. XRD patterns of fresh and the cycled $Li_{1.2}Mn_{0.55}Ni_{0.15}Co_{0.1}O_2$ electrodes in the STD and APTS-containing electrolytes.

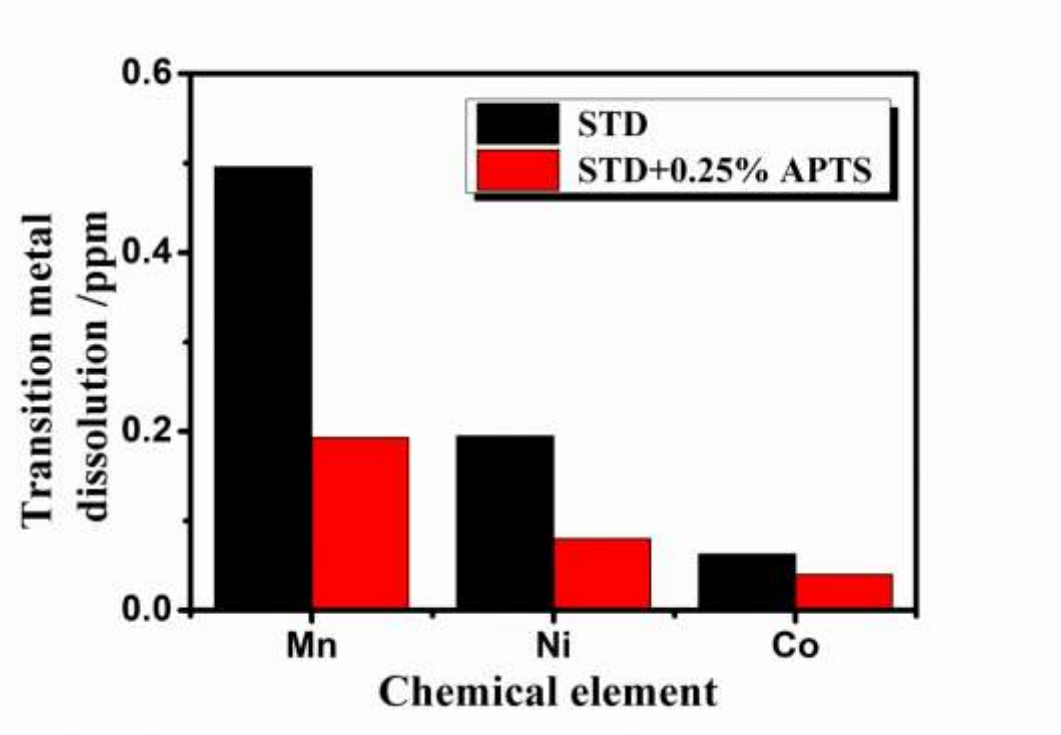

Fig. S7. Deposited transition metal on the Li counter electrode after cycling Li/ $Li_{1.2}Mn_{0.55}Ni_{0.15}Co_{0.1}O_2$ cells in the STD and APTS-containing electrolytes for 300 cycles.

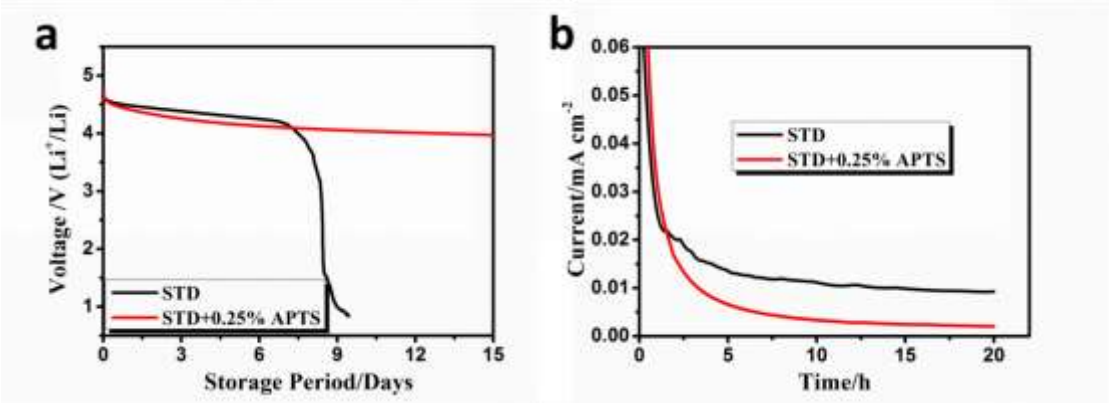

Fig. S8. Voltage decaying curves (a) and chronoamperometric profiles at 4.8 V (b) for charged $Li_{1.2}Mn_{0.55}Ni_{0.15}Co_{0.1}O_2$ electrodes after three charge-discharge cycles at 0.1 C in the STD and APTS-containing electrolytes.

With the protection of interphase constructed by APTS, the LMR electrode can suppress the self-discharge of charge LMR and the electrolyte decomposition. Fig. S8a presents the voltage decaying curves of the charged LMR electrodes after three charge-discharge cycles at 0.1 C in the STD and APTS-containing electrolytes. The voltage of the cell in the STD electrolyte drops dramatically after eight days storage, indicating that LMR suffers severe self-discharge. During the storage of the charged cell, the carbonate electrolytes closing to the surface of electrode is oxidized by the charged LMR, which is accompanied by the reduction of higher valence transition metal ions (Ni^{4+}, Co^{4+} and Mn^{4+}) in LMR, leading to the cell voltage drop.[3] However, the voltage of cell in APTS-containing electrolyte remains stable after storage for fifteen days, indicative of the protection of interphase for LMR. As shown in Fig. S8b, there is a large residual current for the charged LMR electrode in the STD electrolyte under 4.8 V, suggesting that the electrolyte suffers severe decomposition. In the APTS-containing electrolyte, this residual current is reduced significantly, indicating that the interphase constructed by APTS can effectively suppress the electrolyte decomposition.

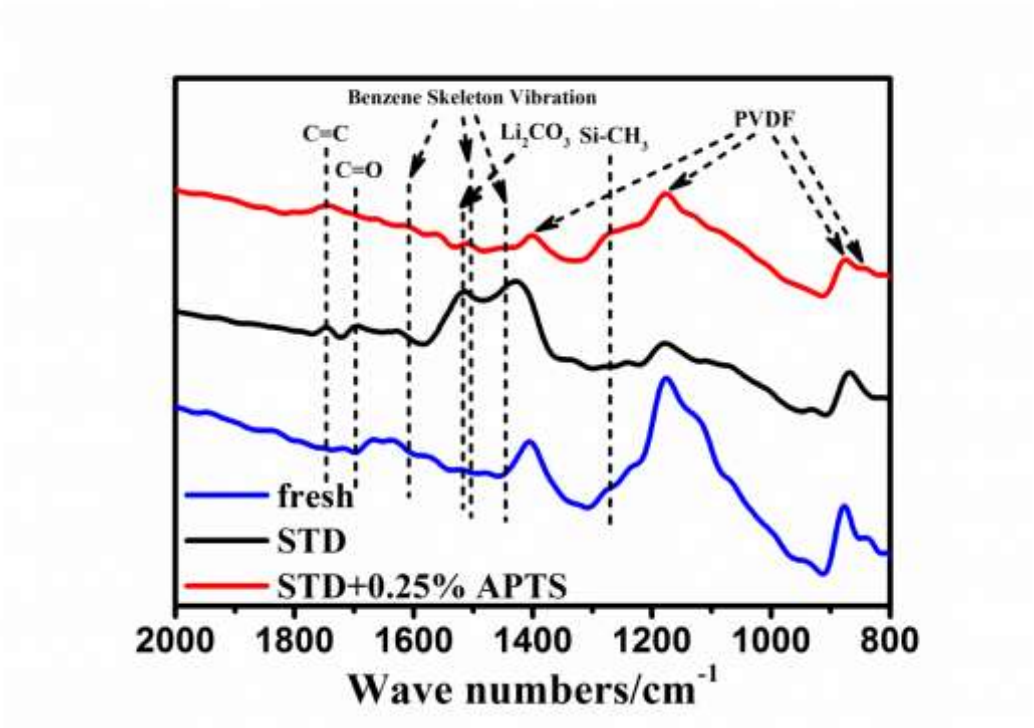

Fig. S9. FTIR spectra of fresh $Li_{1.2}Mn_{0.55}Ni_{0.15}Co_{0.1}O_2$ electrode and the electrodes after cycling test in Fig. 1 for STD and APTS-containing electrolytes.

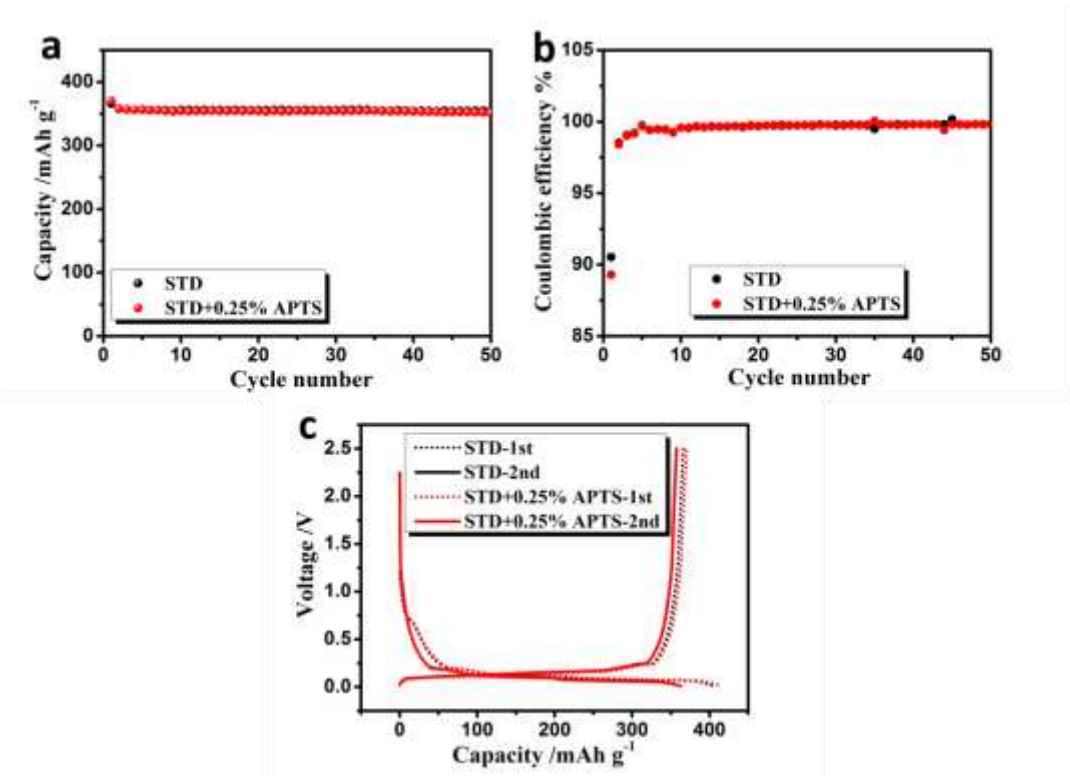

Fig. S10. Cyclic performance (a), corresponding Coulombic efficiency (b) and initial charge-discharge profiles (c) of Li/graphite cells in the STD and APTS-containing electrolytes.

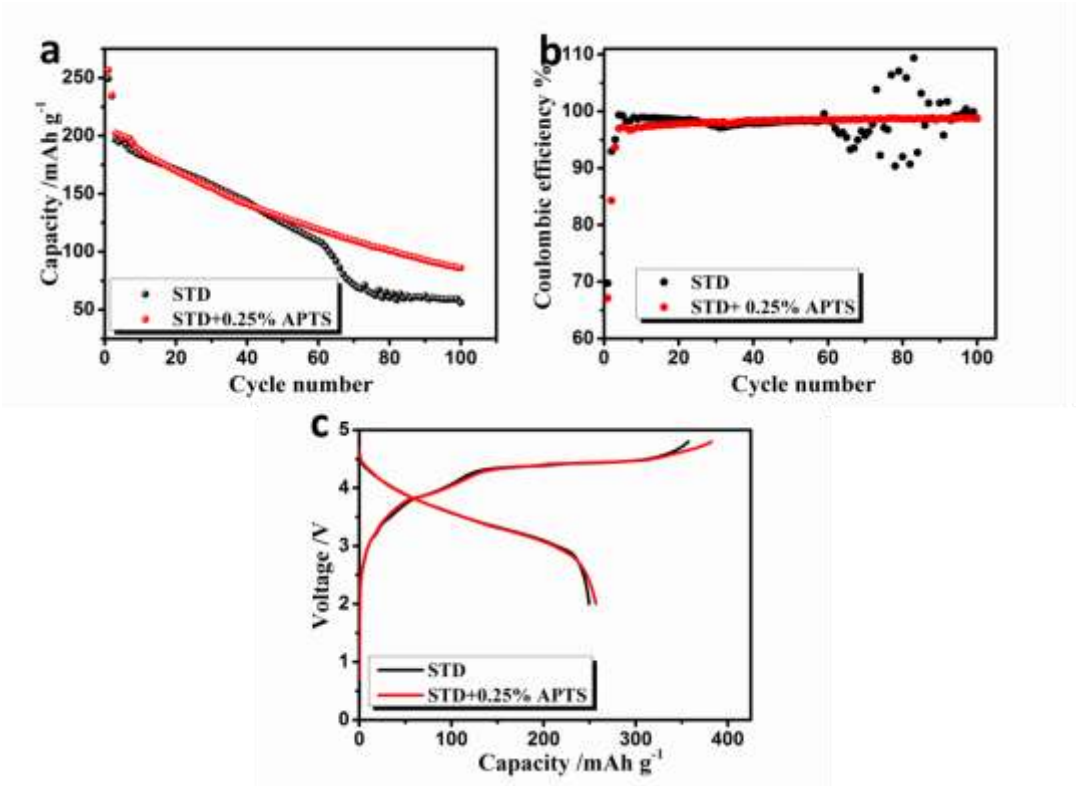

Fig. S11. Cyclic performance (a), corresponding Coulombic efficiency (b) and initial charge-discharge profiles (c) of graphite/$Li_{1.2}Mn_{0.55}Ni_{0.15}Co_{0.1}O_2$ cells in the STD APTS-containing electrolytes.

The $Li_{1.2}Mn_{0.55}Ni_{0.15}Co_{0.1}O_2$/graphite 2025-type coin cells were charged to 4.8 V and then discharged to 2.0 V at 0.1 C (1 C = 200 mA g^{-1}) for initial two cycles and at 0.5 C for following cycles. Although the capacity decay occurs in both electrolytes, the capacity retention in the electrolyte containing 0.25% APTS is 15% higher than that in the STD electrolyte. And the Coulombic efficiency cycled in the STD electrolyte is extremely wobbly in the later period of cycles while stabilized in the electrolyte containing 0.25% APTS. It is noteworthy that the first Coulombic efficiency in the electrolyte containing APTS additive is also lower than that in the STD electrolyte, which implies that APTS also participates in the oxidation reaction in the first charge process. These results reveal that the protective interphase film formed by APTS additive can also suppress the electrolyte decomposition and then improve the cycling stability in the full battery.

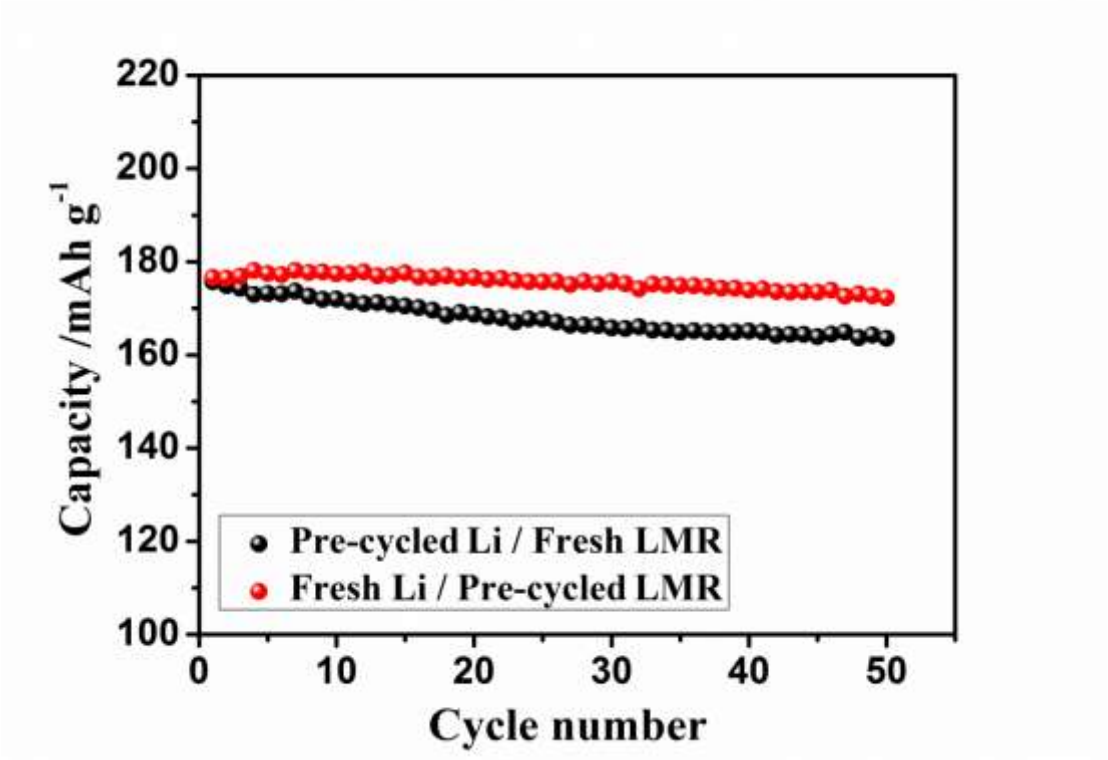

Fig. S12. Cyclic performance of fresh Li/pre-cycled $Li_{1.2}Mn_{0.55}Ni_{0.15}Co_{0.1}O_2$ and pre-cycled Li/fresh $Li_{1.2}Mn_{0.55}Ni_{0.15}Co_{0.1}O_2$ cells in the STD electrolyte at 1C between 2 V and 4.8 V.

The pre-cycled Li and $Li_{1.2}Mn_{0.55}Ni_{0.15}Co_{0.1}O_2$ electrodes were obtained from the Li/$Li_{1.2}Mn_{0.55}Ni_{0.15}Co_{0.1}O_2$ cell after three cycles at 0.1 C in the APTS-containing electrolyte. The fresh Li/pre-cycled $Li_{1.2}Mn_{0.55}Ni_{0.15}Co_{0.1}O_2$ cell exhibits better cyclic stability than the pre-cycled Li/fresh $Li_{1.2}Mn_{0.55}Ni_{0.15}Co_{0.1}O_2$ cell, confirming that the improved cyclic stability of LMR/Li cell by APTS (**Fig. 1**) results from the effect of APTS on LMR cathode rather than Li anode.

References

1. X. Li, T. Gao, F. Han, Z. Ma, X. Fan, S. Hou, N. Eidson, W. Li and C. Wang, *Adv. Energy Mater.*, 2018, **8**, 1701728.
2. P. K. Nayak, T. R. Penki, B. Markovsky and D. Aurbach, *ACS Energy Lett.*, 2017, **2**, 544-548.
3. J. Li, L. Xing, L. Zhang, L. Yu, W. Fan, M. Xu and W. Li, *J. Power Sources*, 2016, **324**, 17-25.